

# The effect of interlayer drying on the ceramic paste extrusion process

Dan Davie<sup>a,\*</sup>, Louis Masters<sup>a</sup>, Matthew Shuttleworth<sup>a</sup>, Pablo Jaramillo Cevallos<sup>a</sup>, James Warren<sup>b</sup>, Jaemin Lee<sup>a</sup>, Robert Kay<sup>a</sup>

<sup>a</sup> School of Mechanical Engineering, University of Leeds, Leeds, LS2 9JT, United Kingdom

<sup>b</sup> Institute of Medical and Biological Engineering, University of Leeds, Leeds, LS2 9JT, United Kingdom

## ARTICLE INFO

Handling Editor: P. Vincenzini

### Keywords:

Paste extrusion  
Drying  
Defects  
Non-destructive evaluation

## ABSTRACT

Paste extrusion (PE) of aqueous ceramic materials can be assisted by layer-wise drying, enabling complex geometries such as overhangs or high aspect ratio (tall and thin) components. However, the removal of water volume causes shrinkage, the effects of which have not previously been studied in the context of PE. In the range of interlayer drying times investigated, a linear relationship between moisture content and shrinkage in the Z direction was found, up to a maximum shrinkage of 6.4 % at a drying time of 90 s, after which further shrinkage was negligible. Shrinkage in the XY plane was also negligible due to the boundary condition of substrate adhesion. In the case of multilayer parts, drying improved the shape accuracy but Z shrinkage was found to cause voids by altering the height and extrudate width in the next layer. The void fraction of complex parts produced with and without shrinkage compensation was found, using  $\mu$ CT, to decrease from 13.3 to 0.6 %. Therefore, this approach can be used to create high-quality components using PE, without necessarily optimising the material formulation for printability, facilitating uptake of novel materials in ceramic additive manufacturing.

## 1. Introduction

Material extrusion of aqueous ceramic pastes; or paste extrusion (PE) involves selective, layer-wise deposition of ceramic paste through a nozzle or orifice. A wide range of particulate materials, including advanced ceramics, have been formulated into printable materials, generally with higher solid loadings than alternative additive manufacturing (AM) methods such as ceramic-loaded stereolithography [1–3]. The high solid loading ensures good particle packing and facilitates the production of high-density components after subsequent thermal processing. As such, PE has been identified as a technique for manufacturing dense, monolithic, technical ceramic components with the increased design flexibility enabled by AM [4]. It has the potential to create next-generation products with applications across a range of high value sectors including electronics, medical, and aerospace [5–8]. To fulfil this potential, certain limitations must be overcome, including issues around dimensional accuracy, resolution, and porosity [4,9]. That is, for widespread adoption of this approach, it must be able to consistently deliver parts meeting the design specifications for shape, dimensions and density.

Typically, designing paste materials with suitable rheological behaviour is critical to this technique. The paste contains ceramic

particles, a suspending agent (water), and a small fraction of organic rheological modifiers. The latter are selected to enable shear thinning rheology to facilitate extrusion, followed by an increase in apparent viscosity and yield stress [3,10,11]. Without this, the printed material would slump under its own weight, reducing the shape accuracy and part quality [11–13]. The development of yield stress has been achieved by adjusting the pH of the suspension, changing the strength of inter-particle forces to give viscoelastic behaviour [12,14,15]. This affords high solid loading but can be challenging and/or time consuming with novel or poorly characterised ceramic compositions. Otherwise, ceramic particles have been suspended within viscoelastic hydrogels [16,17]. This approach is less sensitive to ceramic surface chemistry, but the use of a hydrogel matrix reduces the solid fraction [10]. Either way, optimising the rheological behaviour, a complex product of the material formulation and preparation procedure, is an ongoing challenge to the adoption of PE technologies.

Alternatively, partial drying can be used to develop yield stress in deposited layers as, at high solids loadings, a small change in moisture content causes a steep increase in viscosity and yield stress [18]. This approach maintains a high solid fraction and reduces the reliance on optimising the rheological behaviour, simplifying the material design. However, uncontrolled drying is slow to use layer-by-layer within an AM

\* Corresponding author.

E-mail address: [d.davie@leeds.ac.uk](mailto:d.davie@leeds.ac.uk) (D. Davie).

<https://doi.org/10.1016/j.ceramint.2024.12.499>

Received 28 August 2024; Received in revised form 6 December 2024; Accepted 29 December 2024

Available online 30 December 2024

0272-8842/© 2024 The Authors. Published by Elsevier Ltd. This is an open access article under the CC BY license (<http://creativecommons.org/licenses/by/4.0/>).

method [13]. Alternatively, the drying can be accelerated using a hybrid-AM process, combining AM with an additional energy source [19]. For example, infrared (IR) radiation can be used to increase the temperature of printed material and accelerate the evaporation process [20]. Ghazanfari et al. used interlayer IR drying in a PE process to enable fabrication of complex ceramic components, coining this process Ceramic On Demand Extrusion (CODE)<sup>1</sup> [21].

However, removal of water content from a ceramic body is known to cause proportional shrinkage, the effects of which have not been discussed in the context of PE. Hall et al. [22] report anisotropic sintering shrinkage for piezoelectric samples made using paste extrusion. This was attributed to reduced layer consolidation caused by a drying-induced layer thickness reduction. However, to the best of current knowledge, no dedicated studies exist regarding interlayer drying-induced shrinkage in paste extrusion processes. Indeed, Ghazanfari et al. [23] note that drying is accompanied by a reduction in volume but neglect to study this further as "... the paste cannot shrink at the substrate-paste interface due to adhesion".

Alternatively, information about the drying behaviour during paste extrusion can be found in tape casting literature, by considering the material and geometric similarity of a printed layer and a cast tape. For example, Briscoe et al. studied the drying kinetics of tape cast suspensions, finding that it follows a two-step mechanism, first with an 'external' evaporation-controlled process, followed by an 'internal' diffusion-controlled process. They also note that the thickness of the cast tape decreases in the initial stage as water is removed [24]. Fu et al. studied the effect of formulation parameters on shrinkage and stress development in cast films [25]. Kiennemann et al. studied the drying behaviour, stress development, and factors affecting cracking in tape cast ceramic suspensions, finding that cracking occurs when the maximum stresses are greater than the cohesive forces within the tape [26].

Stresses are generated during drying operations as water is removed, initially from the surface of the material, creating a pressure gradient between the higher-pressure interior and lower pressure exterior [27]. This puts the water in tension, driving flow through the interparticle pore network towards the surface, and corresponding compression on the solid phase, resulting in volumetric shrinkage [28]. However, smaller particles increase this pressure gradient as narrow pores increase the resistance to flow. This can cause non-uniform compressive forces and differential shrinkage of the solid, resulting in defects such as warping and cracking [25,28,29]. Therefore, this study uses micron sized particles to remove the formation of these defects from the experimental hypothesis.

Moreover, this study focuses on the effect of drying-induced shrinkage on the quality of components fabricated using PE; a volumetric process that deposits an exact amount of printed material per layer. The sequential deposition procedure is driven by a toolpath, created parametrically from digital design. Clearly, parameter selection and toolpath optimisation are critical to avoiding defects and are the subject of existing research [30–32]. This novel work presents a toolpath-agnostic method of multi-layer shrinkage characterisation in layer-wise-drying assisted PE. The effect of shrinkage on macrostructural density is observed and adjusted for using changes to toolpath parameters. This approach aligns with Industry 4.0, improving part quality by intelligent machine operation, saving time and costs associated with optimising novel materials for PE.

<sup>1</sup> Note that, in research, ceramic paste extrusion has been called Robocasting (RC), Direct Ink Write (DIW), CODE, and more [10,18,21,36]. The feedstock is sometimes referred to as a paste, ink, or slurry. For consistency, the terms paste, and paste extrusion will be used throughout this work.

## 2. Materials and experimental methods:

### 2.1. Apparatus and materials

#### i. Preparation of Aqueous Ceramic Paste

The paste contained Aluminium Oxide (Alumina, Al<sub>2</sub>O<sub>3</sub>, 99.8 %, d50 = 2.5–5.0 μm, Ferro Co., USA) powder with 1 wt% Manganese Dioxide (MnO<sub>2</sub>, Fischer Chemical, USA) and 1 wt% Titanium Dioxide (TiO<sub>2</sub>, 98+ %, Thermo Scientific, USA) as sintering aids, recommended by Gnana-sagaran et al. [33]. 5 wt% of a proprietary, pseudo-cationic dispersant was dissolved into de-ionised water using a magnetic stirrer (AREC.X, VELS Scientifica, Italy) at ambient temperature. The powders were transferred into this solution and mixed using a planetary mixer (ARE-250, Thinky Co., Japan) for 3 min at 1500 rpm to homogenise the mixture and break up soft agglomerates. 1 wt% commercially available, cellulose-based binder was added to the slurry and re-mixed before degassing for 3 min at 1500 rpm. The paste was then loaded into the cartridge and degassed again to remove air pockets. Then, the cartridge was loaded into the PE apparatus. The resulting paste had a solid loading of 75.6 wt%, or 43.7 vol%.

The paste composition was determined through a series of coarse trials to determine the moisture content required for extrudability. The rheological behaviour was not 'optimised' since this work aims to demonstrate an alternative method to improve printability, using interlayer drying. However, the rheological behaviour is relevant during drying operations and a flow characterisation curve is available in the supplementary material.

#### ii. Paste Extrusion Apparatus and Software

Extrusion of the alumina paste was performed using a custom-built ceramic PE apparatus, see Fig. 1. This combined additive (PE) and assistive processes onto a 3-axis motion platform, with in-situ monitoring capabilities [34]. The PE process used a stepper motor driven ram extruder to enable volumetrically controlled extrusion. The maximum extrusion rate, limited by the ram's torque, was fixed at 15 mm<sup>3</sup>s<sup>-1</sup>. An auger screw shearing valve was used to control the start/stop of material delivery, improving the extrusion response rate as described in Refs. [35, 36]. The speed of the auger screw was tuned to achieve consistent extrusion and accurate layer height, the average speed was ~2.4 revolutions per second. The extruder was fitted with a luer-lock straight-walled metal nozzle (1.37 mm diameter, Adhesive Dispensing Ltd, UK). The nozzle toolpath was controlled by GCODE which was prepared, using constant parameters, in SuperSlicer [37] and compiled in Python.

The apparatus was fitted with an IR lamp (300 W, RS Components, UK), fixed 75 mm above the layer surface during drying. It was noted that the temperature of the aluminium build plate increased during drying, so the plate was cooled back to 25 °C between tests. The experiments were performed within a humidity controlled (±5 %) laboratory environment, and local extraction was used to ensure sufficient air circulation. The in-situ monitoring system included a strip laser profilometer (scanCONTROL 2900-50, MicroEpsilon, Germany) to measure the part dimensions and a top-down camera (VCXU.2–201M.R, Baumer Vision Technologies, Switzerland) with telephoto lens (V1226-MPZ, Computar Global, Japan) for visualisation. Laser and camera data acquisition was automated using Python.

### 2.2. Experimental methods

The experimental work for this paper was divided into independent objectives to help better understand the drying and shrinkage behaviour and their influence on part quality. Multilayer parts were fabricated to assess the relationship between interlayer drying time, moisture content, and part quality. Single layer samples were produced to measure the change in layer dimensions due to interlayer drying. This was done

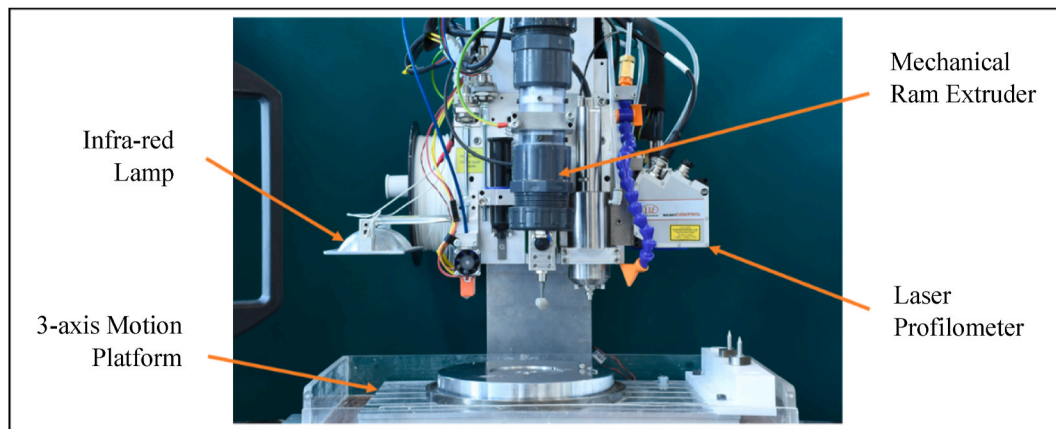


**Fig. 1.** The custom-built paste extrusion apparatus including high viscosity paste extruder, infra-red lamp, 3 axis motion platform and a laser profilometer. (For interpretation of the references to colour in this figure legend, the reader is referred to the Web version of this article.)

as it ensures a rigid substrate and known layer height, removing these as variables.

Parts were dried using interlayer drying times of [0, 15, 30, 45, 60, 75, 90, 105] s. These time scales were selected based on scoping experiments, which showed that no further shrinkage occurred after 105s. Also, they are comparable to other stages in the paste extrusion process, e.g., the time to print a layer. Generally, the printing regime was as follows: print layer, dry for drying time, capture image, repeat until end.

- i. Moisture content and part quality as a function of interlayer drying time.

Cylindrical parts, with diameter 25 mm and height 9 mm, were printed with each drying time. Each cylinder comprised of 15, 0.6 mm thick layers, with one external perimeter and rectilinear infill. This shape was chosen to avoid non-uniform drying at vertices. Using the laser, the part was scanned every layer after drying. Analysis of the laser data is detailed in Section 2.3. Upon completion of the part, the final build plate temperature was recorded, and the part was immediately transferred to the moisture analyser (PMB-163, Adam Equipment, UK, Heating: Single/120 °C, Interval: 20 s, Stop: Stable/0.001g/90 s). Three repeats were conducted for each drying time. Tests were conducted in a random order, with one repeat per batch of material.

- ii. Dimensional changes as a function of interlayer drying time.

Single layer samples of the cylinders described above were printed at each drying time. Layers with defects were discarded and repeated to ensure the data represents the shrinkage of fully dense layers only. The layer was scanned before and after drying, and the relative shrinkage in the Z direction,  $\Delta Z$  was calculated as a percentage using Equation (1). Here, Z represents the modal height of the printed surface (see Section 2.3), ‘wet’ and ‘dry’ refer to before and after drying, respectively. Twelve repeats were conducted for each drying time across three batches of material. The tests were completed in a random order.

$$\Delta Z = \frac{Z_{\text{wet}} - Z_{\text{dry}}}{Z_{\text{wet}}} \times 100 \% \quad (1)$$

### 2.3. Laser data capture and processing

In the raw laser data, the part surface was represented by a series of line scans, see Fig. 2a. The laser scanner was positioned ~70 mm from the build plate. At this position, the 1260 data points in the line covered 59.6 mm on the build plate, giving a resolution of ~0.045 mm in the Y direction. In the X direction, a scan was taken every 0.5 mm. From the data sheet, the resolution in the Z direction is ~0.004 mm. Edges of the

part in a scan were detected using the ruptures Python package (ruptures.window, model: 12, window length: 100), see Fig. 2b. The portion between the change points represented the part surface, see Fig. 2c. The X and Y coordinates of the change points were input to a circle fitting algorithm (circle\_fit.taubinSVD) to estimate the layer diameter.

Z coordinates from the surface data were used as a 1-dimensional dataset to isolate the primary mode of shrinkage, reported in literature as a reduction in the thickness (Z) direction [24,29]. This approach removes toolpath effects, such as the surface texture shown in Fig. 2b, and enabled analysis of very large datasets by reducing computational load. Furthermore, the accuracy of the realised geometry to the digital design can be described by statistical metrics such as mode, standard deviation, and skew, which are taken as key indicators of layer quality. These metrics were calculated using a gaussian estimation of the probability density function (scipy.stats.gaussian\_kde). The modal value represented the average height of a printed layer. The standard deviation represented the flatness. The skew indicated the height of outlying data points (defects).

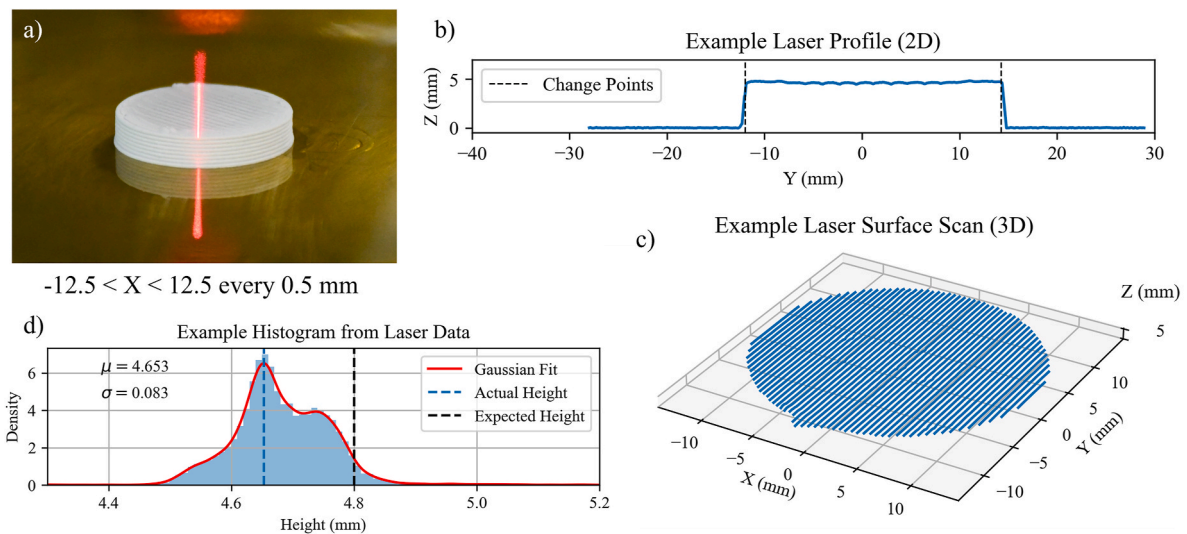
Histograms were plotted for visualisation. An example plot of a single layer scan is shown in Fig. 2d. The peaks at Height  $\approx$  4.75 and 4.65 mm represent the peaks and troughs of the surface texture shown in Fig. 2b. However, the overall part quality, across multiple layers<sup>2</sup> and repeats, was presented by combining the height data into a single dataset for each drying time. These combined histograms tend towards a normal distribution due to the central limit theorem [38], reducing noise from defects while still capturing the data, and highlighting general trends.

## 3. Results and discussion:

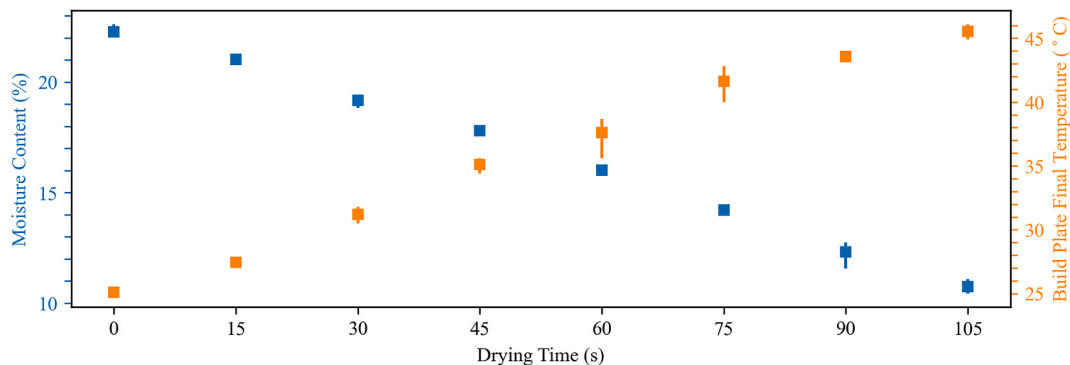
- i. Moisture content and part quality as a function of interlayer drying time.

Fig. 3 shows an increase in final build plate temperature and a decrease in moisture content as the interlayer drying time increases. As the part (and the plate) heats up under the IR lamp, the part begins to dry and the moisture content decreases. Fig. 3 indicates a linear relationship between moisture content and drying time between 0 and 105 s. For example, there is a ~6% decrease from 23 to 17% over the first 60 s of drying. The linear relationship suggests that the evaporation rate was independent of the moisture content; the drying was progressing in the constant rate period, as explained by Ford [20]. During the constant rate

<sup>2</sup> For multi-layer samples, the data was presented as height error, calculated by subtracting the expected layer height from the surface height data.



**Fig. 2.** The stages during the capture and processing of laser data. Fig. 2a shows the laser profilometer positioned over a cylindrical part. Fig. 2b shows an example laser profile. Fig. 2c shows the surface of the part from 2a represented by a series of line scans. Fig. 2d shows the surface height data from 2c plotted as a histogram, highlighting the Gaussian fit curve, layer height,  $\mu$ , and standard deviation,  $\sigma$ .



**Fig. 3.** The effect of interlayer drying time on the final build plate temperature and measured moisture content of printed parts.

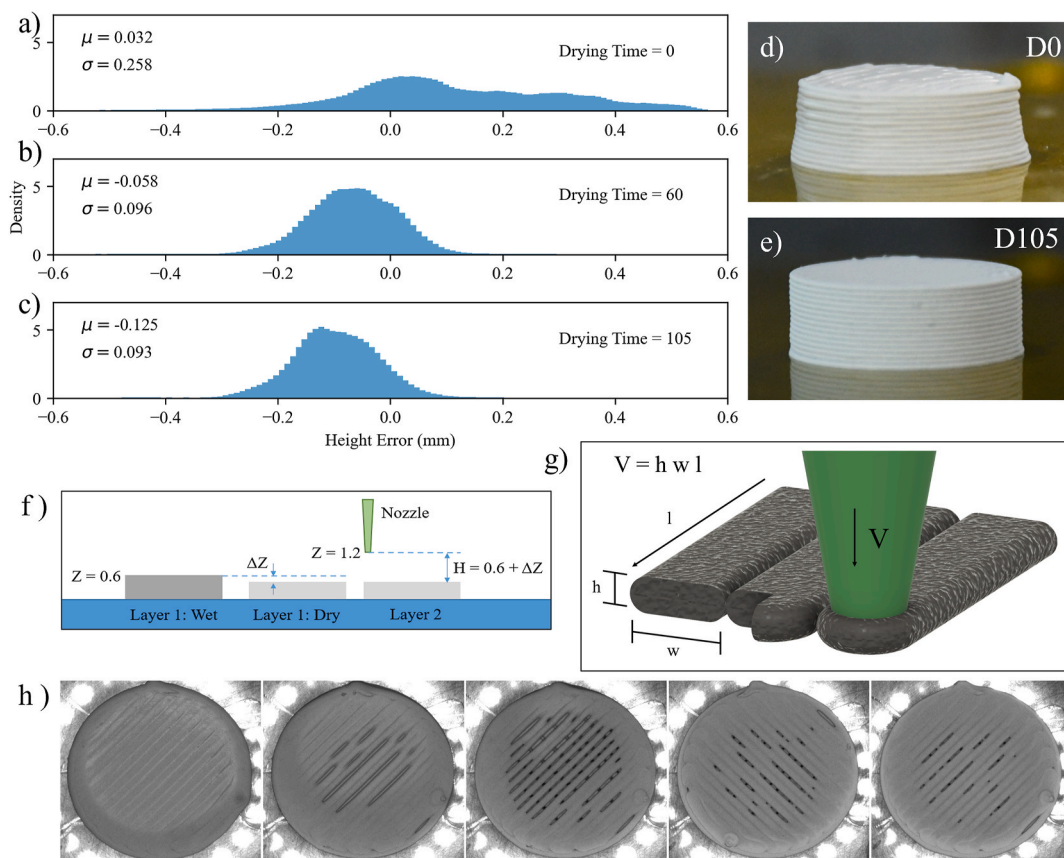
period, the surface behaves as a free water surface. As evaporation occurs, water flows from the interior of the part at a sufficient rate to keep the surface wet. This is the ‘external’ evaporation-controlled drying stage in the findings of Briscoe *et al.* [24]. During this stage, the volumetric shrinkage is equal to the volume of water evaporated. The shrinkage is due to a reduction in the thickness of an interparticle film of water which; initially, was lubricating particle-particle contacts, enabling flow during deposition.

Fig. 4 shows the relationship between drying time, height error and part quality, using example combined histograms (15 layers x 3 repeats) for drying times of [0, 60, 105] s. Fig. 4a shows that, when the drying time was low, the standard deviation was large, the printed surface was typically uneven. During PE, material is usually extruded onto a rigid substrate which causes the extrudate to spread to the appropriate width. In this case, the yield stress of the previous layer was insufficient to resist deformation under the force of the extruded material, meaning the extrudate did not spread to the desired width, leaving uncontrolled voids in the printed layer. Fig. 4d shows poor shape accuracy with the part walls sloping outwards at the bottom. However, Fig. 4a shows the modal height error is greater than zero, suggesting the sloping walls were not caused by slumping. Instead, the parts appeared to contract upwards and inwards. In fact, the part diameter decreased by 0.7 mm over the first 7 layers, perhaps driven by residual tensile stresses in the extrudate.

Fig. 4b and c shows that increasing the interlayer drying time

decreased the variance in the height data. As the moisture content (and particle mobility) decreased, the viscosity of the paste increased and a yield stress developed, allowing the layer to act as a rigid substrate to support the subsequent layer. Fig. 4e shows a cylindrical part, the shape accuracy improved when interlayer drying was used. However, Fig. 4b and c shows that the modal height decreased, becoming negative, with increasing drying time. The layer surface was below the expected height due to drying-induced shrinkage. This caused an increase in the effective height of subsequent layers (see Fig. 4f). An increase in effective layer height ( $h$ ) caused a reduction in extrudate width ( $w$ ) since the length of the line ( $l$ ) and volume of material delivered ( $V$ ) was constant (controlled by GCODE), see Fig. 4g. This results in the formation of voids in the printed layer as the extrudate volume was insufficient and did not spread to the desired width, see Fig. 4h. The formation of such voids means the standard deviation in measured height does not tend to zero, but some minimum  $\sim 0.09$  mm (see Fig. 4c).

Notably, cracking was not observed in any of the samples produced in this work, despite being a common problem when drying ceramic artefacts using IR radiation [25,26]. Ford [20] explains that linear travel of radiation and high energy transfer rates prevent the use of IR drying with complex geometries as uneven heating/drying rates are likely to cause cracks. However, in this case, the layer-wise method means that each drying object approximates a thin film, regardless of final part geometry. Additionally, the absence of cracking suggests that the material formulation and drying configuration used in these experiments



**Fig. 4.** a, b, c) show combined histogram plots for each layer and repeat printed with a drying time of 0, 60, 105 s, respectively. Fig. 4d and e) shows example side profiles of cylindrical parts dried with 0 and 105 s of drying, respectively. Fig. 4f) A schematic to show the conservation of volume in a paste extrusion process, demonstrating the effect of increased layer height on extrudate width. Fig. 4g) shows top-down images of layers 1, 3, 5, 10, 15 of a sample part made with 45s of drying per layer, showing the formation of voids because of decreased extrudate width.

were appropriate for use in drying assisted PE, e.g., the green strength is greater than the stresses developed in the part as it dries [26].

ii. Dimensional changes as a function of interlayer drying time.

The single layer samples produced higher quality layers than the multi-layer samples. The modal layer height across all the single layer scans (96 in total) was 0.602 mm, with a standard deviation of 0.053 mm before drying. Fig. 5 shows the relative shrinkage of single layer samples, as a function of drying time. Shrinkage in the XY direction is negligible, in agreement with the Ghazanfari et al. [23]. Adhesion to the build plate constrained the material in the XY plane. Particle movement

within the plane was also restricted by the thin film geometry and high viscosity of the material. Additionally, there was no driving force for transport within the XY plane. However, the upper surface was unconstrained, the vertical transport of water to replenish the free water surface caused the ceramic mass to travel downwards.

Fig. 5 shows shrinkage in the thickness (Z) direction was not negligible. The shrinkage was slow in the first 0–15 s of drying as the temperature was still increasing, accelerating the drying rate. Then, the shrinkage increased between 15 and 90 s of drying before slowing to zero after 90 s. This effect is responsible for the height error and void formation shown in Section 3i.

Initially, each ceramic particle is surrounded by a film of water (and

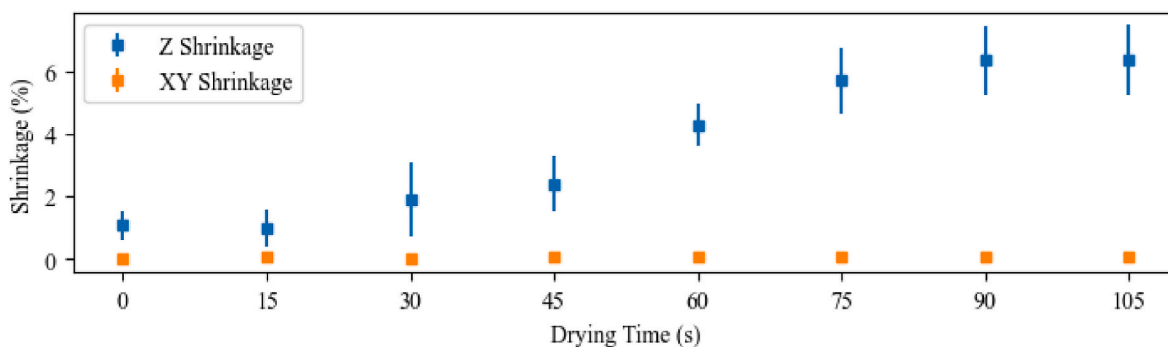


**Fig. 5.** Shrinkage in the Z (thickness) and XY (planar) directions as a function of interlayer drying time. Shrinkages are presented as a percentage, relative to the initial dimension.

additives) adsorbed to the particle surface. As the moisture content decreases, the thickness of the interparticle film decreases. During this period, a linear relationship between water content and shrinkage is expected [20]. At some point, in this case after 90 s of drying, the thickness of the interparticle film becomes zero; the particles are in contact. After this, the remaining water content is held in a network of pores between particles, and no further shrinkage occurs. This is demonstrated by the levelling of the curve between 90 and 105 s in Fig. 5. The maximum measured shrinkage was 6.4 %. It should be noted that the magnitude of shrinkage and the time-to-dry will depend on material parameters such as initial water content and organic composition. Therefore, the magnitude of shrinkage results from this study are material specific and should not be used with alternative paste compositions.

#### 4. Validation: the effect of interlayer drying on part quality:

##### i. Methods

Larger parts with more complex geometry were printed to visualise the effect of drying with and without shrinkage compensation on the quality of a functional product; a bracket - with arbitrary dimensions, given in Fig. 6. This was chosen to highlight the freeform nature of AM, including upright and overhanging geometry. Laser scanning was performed within the region AA indicated in Fig. 6, as the holes in the bracket part would have caused issues for the edge detection algorithm outlined in Section 2.3. Three examples of the part were made, details are given in Table 1.

A drying time of 60 s was deemed sufficient to preclude slumping based on results from section 3.i. The shrinkage at 60s of drying was measured at 4.3 %, according to Fig. 6. This value was used to adjust the Z coordinates of each layer in GCODE by Equation (2). The part was initially scaled in the Z direction by 4.3 % to preserve the final dimensions.

$$Z_n = nH - \frac{H\Delta Z}{100} (n - 1) \quad (2)$$

$Z_n$  is the Z coordinate of the  $n$ th layer,  $n$  is the layer number, and  $H$  is the layer height. The  $nH$  term represents the initial layer height before scaling.  $\Delta Z$  is the shrinkage in the Z direction expressed as a percentage. This was converted to an absolute shrinkage and subtracted from every layer height except the first layer, hence  $(n - 1)$ .

To study the effect of interlayer drying and shrinkage compensation on finished ceramic components, the parts were sintered in a box furnace (RHF 1600, Carbolite Gero, UK) at 1500 °C for 2 h. The samples were imaged using a micro-Computed Tomography ( $\mu$ CT) scanner (XtremeCT, Scanco Medical AG, Switzerland, Current: 114  $\mu$ A, Integration time: 300 ms, Voltage peak: 70 kV) at an isotropic resolution of 82  $\mu$ m to observe the post-sintering fabrication porosity. Image segmentation was performed using Simpleware ScanIP (2021.03, Synopsis,

**Table 1**

details the drying time and shrinkage compensation used to produce three sample parts, A, B, and C.

Part Name	Interlayer Drying Time (s)	Shrinkage Compensation (%)
A	0	–
B	60	–
C	60	4.3

USA). The total and empty volumes were calculated to quantify the void fraction of each sample.

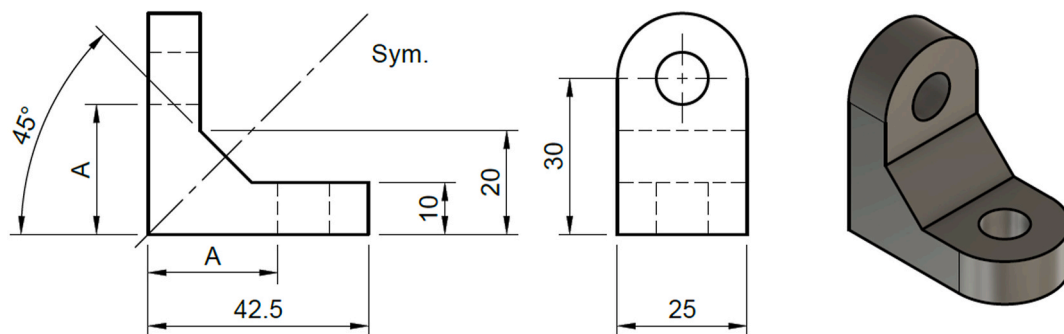
##### ii. Results and Discussion

Fig. 7 shows examples of top-down images (12th layer) and an isometric view of the sample parts. Fig. 7a shows poor shape accuracy and layer quality when interlayer drying is not used. The shape accuracy also decreases above  $Z \approx 21$  mm because the time between layers decreased when laser scanning was stopped. This indicates that although the material was printable, the rheology was not suitable for PE with ambient drying. Fig. 7b shows improved shape accuracy when interlayer drying is used, including successful realisation of an unsupported overhang. However, many voids are present in the top-down image due to shrinkage related underextrusion. Fig. 7c shows that the number of voids decreased when shrinkage compensation was used, as a greater volume of material is deposited in the same volume of part.

Results from the  $\mu$ CT scanner confirm that the density of part C is greater than part B. Quantitative results from the segmentation of  $\mu$ CT data are shown in Table 2. To reduce scan time, part A was not scanned as this part would be classed as a failure due to the poor shape accuracy. A sample slice (82  $\mu$ m thickness) of the parts B (left) and C (right) is shown in Fig. 8. Voids shown in Fig. 7b are still present after sintering and are shown clearly in Fig. 8.

Table 2 shows that the empty volume decreased from 2.1 to 0.6 % when shrinkage compensation was used. However, the total volume of part B is also significantly smaller than that of part C, despite being produced with almost identical dimensions. During removal from the build plate, a section of material fractured from the base of part B because the first few layers contained voids and were not strong enough to withstand build plate removal without fracture. This section is encircled in Fig. 8b. Accounting for this lost volume, the empty volume in part B is calculated (based on part B having the same total volume as part C) as 13.3 %. Regardless of empty volume, the fracture would classify part B as a failure. Nonetheless, the  $\mu$ CT data confirms that the internal void fraction can be reduced by compensating for drying-induced shrinkage during accelerated, interlayer drying.

Additionally, scaling a part before slicing and adjusting the Z coordinates in this manner is liable to alter the part dimensions; the final Z coordinate was 34.2 and 34.5 mm for parts B and C, respectively. A better approach would be to compensate for shrinkage by increasing the



**Fig. 6.** Dimensions of a part used to demonstrate the effect of interlayer drying with shrinkage compensation on a functional product. Section AA represents the region captured in laser data.

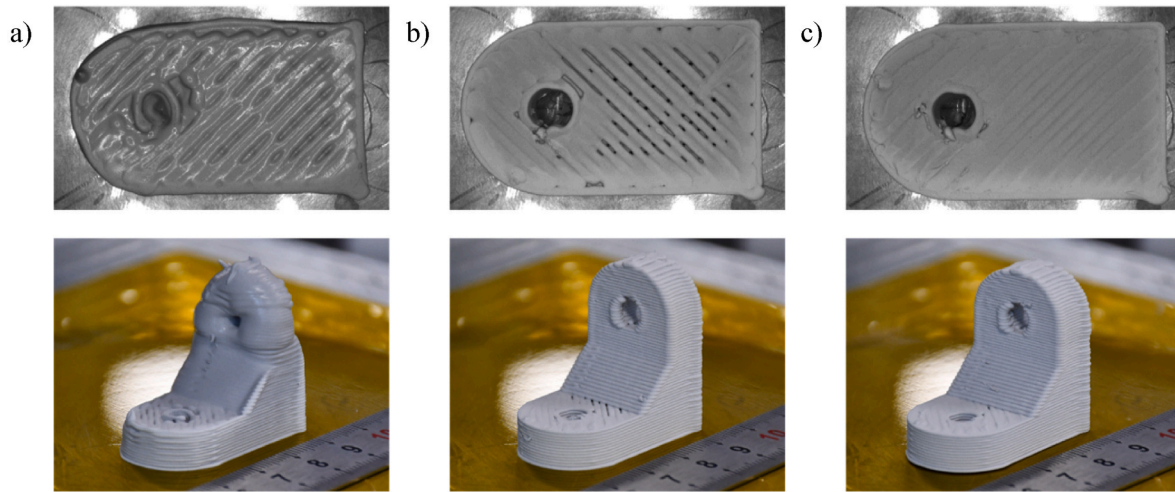


Fig. 7. The quality of parts fabricated using 0 s of interlayer drying. Showing a top-down view of the base of the part (top) and an isometric view (bottom). Fig. 7a, b, c correlate to part A – no drying, part B – 60 s of interlayer drying, and part C – 60 s of interlayer drying with 4.3 % Z compensation, respectively.

Table 2

Results from the segmentation of the  $\mu$ CT scan showing the total and empty volumes of the parts.

Part	Total Volume (mm <sup>3</sup> )	Empty Volume (mm <sup>3</sup> )	Empty Volume (%)
B	4816.6	103.4	2.1
C	5437.4	33.9	0.6

extrusion multiplier, depositing more material per extruded line. Furthermore, measuring the height of each layer in-situ and dynamically adjusting the extrusion multiplier would account for any shrinkage variation associated with changes in layer height, geometry, distance to build plate, material variability. This approach requires closed-loop control which is not always supported by additive manufacturing firmware but will be the subject of further study. Current users of interlayer drying-assisted PE processes, without access to a laser profilometer, should increase the extrusion multiplier to some material-specific value that can be found using trial and error.

Additionally, the time taken to print a part,  $t$  increases when interlayer drying is used by Equation (3).

$$t = t_0 + N (t_{drying}) \tag{3}$$

Where  $t_0$  is the original print time,  $N$  is the total number of layers and  $t_{drying}$  is the interlayer drying time. For example, the print times increased between parts A, B, and C. They were 46, 102, and 105 min, respectively. However, the post-shaping drying time (and shrinkage) would be reduced, and part quality indicators such as the shape accuracy and part density were improved, suggesting an overall increase in manufacturing efficiency despite the increase in print time.

### 5. Discussion: generation and implementation of a model layer:

During the experimental work outlined in Section 2.ii. and 3.ii., 96 single layer samples without defects were printed and analysed. This meant that the laser data from the 96 samples could be used to create a model layer, a standard for acceptable layer quality. In theory, an ideal layer would appear as a single bin on the histogram plot at the expected layer height. This was not achieved in practice.

Combined datasets from all the single layer experiments are shown in Fig. 9. The modal surface height of the wet layers was 0.602 mm, which suggests the extrusion process overall is accurate given the intended layer height of 0.600 mm. In this case, the laser scans from every dry layer (with different drying conditions) are combined into a single plot, hence the dry modal height is not meaningful. The standard deviation of the wet and dry layers was 0.053 and 0.051 mm, respectively, suggesting that interlayer drying tends to increase the flatness of the layer. This is likely due to capillary forces acting to normalise surface texture. Additionally, the dry layer data appears to be normally distributed. This indicates that the expected quality of a layer produced using PE could be predicted using a normal distribution curve with modal height,  $\mu$  = expected layer height, and standard deviation,  $\sigma$  = 0.05 mm. The absolute value of 0.05 mm may be dependent on the layer geometry, however more data would be required to confirm this.

In this work, the dry data series was normalised about zero and used as an indicator of layer quality for the parts produced in Section 4. Fig. 10a shows a combined histogram plot containing laser data from every layer surface. The surface height data of part A has a high variance and is negatively skewed, the yield stress is insufficient to support the mass of printed material and slumping occurred. This differs from the data in Fig. 4a because the mass of printed material was greater, and

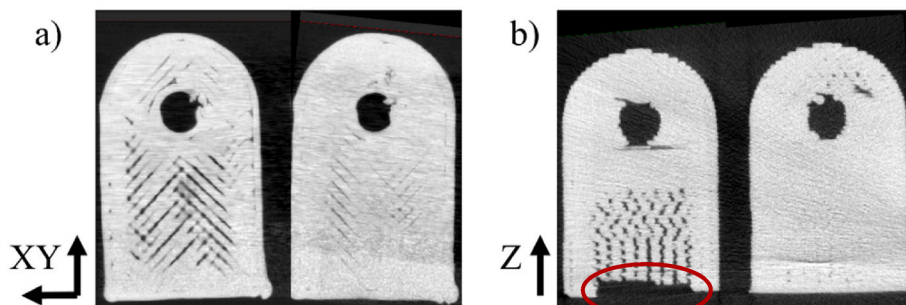


Fig. 8. a, b) shows sample slices taken from a  $\mu$ CT scan of the sintered parts B (left) and C (right), in the XY and Z directions, respectively.

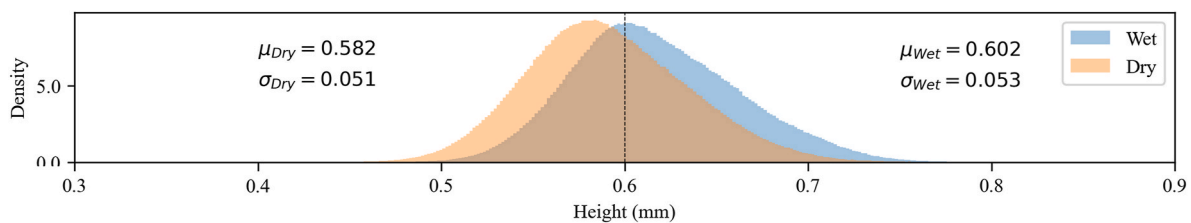


Fig. 9. Aggregate model layer created by combining height datasets from 96 single layer samples before and after drying.

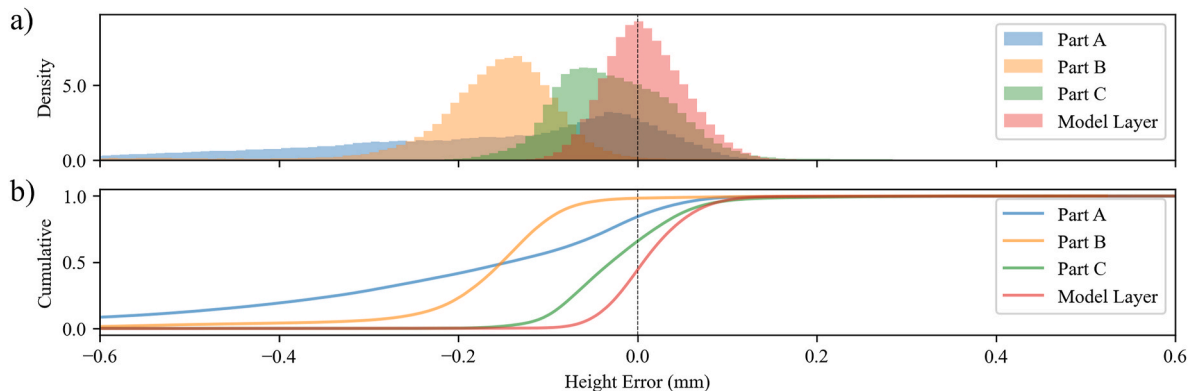


Fig. 10. a. Histogram containing height data from every layer of parts A, B, C, and a model layer, to show the effect of interlayer drying on the paste extrusion process. Fig. 10b shows the same data on a cumulative frequency plot for an alternative view.

slumping was the dominant behaviour. Part B shows decreased variance, but the height error is large and negative due to drying induced shrinkage. Part C shows reduced height error, but it is still more negative than expected. This suggests that the layers shrink more than the compensated value of 4.3 %. Given the repeated exposure to IR radiation and increasing build plate temperature, multilayer parts would shrink more than single layers, up until the maximum measured shrinkage of 6.4 %. However, accurately measuring the shrinkage of a multilayer part is challenging because production of a dense nth layer with accurate layer height relies on knowing the height of the previous layer, strengthening the argument for closed loop control and dynamically adjusted print parameters. Additionally, interlayer drying past the point of maximum shrinkage could preclude any post-shaping drying shrinkage, facilitating the fabrication of dimensionally accurate components. However, measurement of part dimensions before and after final drying, not captured in the present study, would be required to confirm this.

Fig. 10b shows the laser surface data from Fig. 10a as a cumulative frequency plot. A part with ideal print quality would appear overlaid onto the model layer curve. That is, the quality of the printed component is indicated by the steepness of the curve, and 180° rotational symmetry about (0, 0.5). Therefore, Fig. 10 shows that interlayer drying with shrinkage compensation can be used to improve the quality of parts fabricated by ceramic paste extrusion. This statistical approach could be implemented by closed-loop control algorithms in smart machinery and used to decrease the time and costs associated with optimising novel ceramic paste formulations for PE.

## 6. Conclusion

This work shows that interlayer IR drying can improve the shape accuracy of ceramic parts fabricated using the paste extrusion process when the paste rheology is not optimal. Interlayer drying reduces the water content of a printed layer, increasing the yield stress and rigidity of a printed layer. However, the reduction in water content also decreases the volume. The thin film geometry and direction of mass

transport mean that this shrinkage is constrained to the thickness (Z) direction. This increases the effective layer height of subsequent layers and leads to under extrusion effects such as voids, decreasing the macrostructural density. The drying shrinkage was characterised and used to adjust Z coordinates in GCODE for a functional part, compensating for the reduction in layer thickness. This reduced the number of voids in the printed component, increasing the density, which was confirmed using  $\mu$ CT, where the empty volume was found to decrease from 13.3 to 0.6 %. However, uncertainty in the final dimensions after scaling the part in the Z dimension suggests that such an approach is not optimal. An alternative approach would be to measure the surface height of dried layers in-situ and dynamically adjust the extrusion multiplier, increasing the volume of material deposited in the subsequent layer. This method would also be robust to local variation in material formulation, layer parameters such as shape or thickness, and will be the subject of future study.

Finally, combining the surface data from the single layer samples allowed a model layer to be generated. This suggested that the surface height data could be expected to take a normal distribution about the expected layer height with standard deviation of 0.05 mm. Parts fabricated in this work were compared to the model layer, indicating that the part quality increased when interlayer drying with shrinkage compensation was used. As such, this approach can be used within the paste extrusion process to improve the print quality without necessarily optimising the paste rheology. Adoption of this approach could expedite the uptake, and increase the workable envelope, of materials in ceramic paste extrusion processes.

## CRediT authorship contribution statement

**Dan Davie:** Writing – original draft, Visualization, Validation, Software, Project administration, Methodology, Investigation, Data curation, Conceptualization. **Louis Masters:** Writing – review & editing, Software, Methodology, Conceptualization. **Matthew Shuttleworth:** Writing – review & editing, Supervision, Resources, Methodology, Conceptualization. **Pablo Jaramillo Cevallos:** Writing – review &

editing, Conceptualization. **James Warren:** Visualization, Formal analysis, Data curation. **Jaemin Lee:** Supervision, Conceptualization. **Robert Kay:** Writing – review & editing, Supervision, Project administration, Funding acquisition, Conceptualization.

### Code availability

The data and code used to obtain the results in this paper are available at <https://doi.org/10.5518/1567>.

### Declaration of competing interest

The authors declare the following financial interests/personal relationships which may be considered as potential competing interests: Dan Davie reports a relationship with Hydra Manufacturing Ltd that includes: employment and equity or stocks. Louis Masters reports a relationship with Hydra Manufacturing Ltd that includes: employment and equity or stocks. Matthew Shuttleworth reports a relationship with Hydra Manufacturing Ltd that includes: employment and equity or stocks. Robert Kay reports a relationship with Hydra Manufacturing Ltd that includes: employment and equity or stocks. If there are other authors, they declare that they have no known competing financial interests or personal relationships that could have appeared to influence the work reported in this paper.

### Acknowledgements

This work has been funded thanks to the Engineering and Physical Sciences Research Council, UK Case Scholarship EP/T517860/1.

### Appendix A. Supplementary data

Supplementary data to this article can be found online at <https://doi.org/10.1016/j.ceramint.2024.12.499>.

### References

- [1] L. Rueschhoff, W. Costakis, M. Michie, J. Youngblood, R. Trice, Additive manufacturing of dense ceramic parts via direct ink writing of aqueous alumina suspensions, *Int. J. Appl. Ceram. Technol.* 13 (2016) 821–830, <https://doi.org/10.1111/IJAC.12557>.
- [2] A.U. Khan, B.J. Briscoe, P.F. Luckham, Evaluation of slip in capillary extrusion of ceramic pastes, *J. Eur. Ceram. Soc.* 21 (2001) 483–491, [https://doi.org/10.1016/S0955-2219\(00\)00213-2](https://doi.org/10.1016/S0955-2219(00)00213-2).
- [3] J.A. Lewis, Colloidal processing of ceramics, *J. Am. Ceram. Soc.* 83 (2000) 2341–2359, <https://doi.org/10.1111/J.1151-2916.2000.TB01560.X>.
- [4] Y. Lakhdar, C. Tuck, J. Binner, A. Terry, R. Goodridge, Additive manufacturing of advanced ceramic materials, *Prog. Mater. Sci.* 116 (2021) 100736, <https://doi.org/10.1016/J.PMATSCI.2020.100736>.
- [5] A.M. Stanciuc, C.M. Sprecher, J. Adrien, L.L. Roiban, M. Alini, L. Gremillard, M. Peroglio, Robocast zirconia-toughened alumina scaffolds: processing, structural characterisation and interaction with human primary osteoblasts, *J. Eur. Ceram. Soc.* 38 (2018) 845–853, <https://doi.org/10.1016/J.JEURCERAMSOC.2017.08.031>.
- [6] J.S. Pelz, N. Ku, M.A. Meyers, L.R. Vargas-Gonzalez, Additive manufacturing of structural ceramics: a historical perspective, *J. Mater. Res. Technol.* 15 (2021) 670–695, <https://doi.org/10.1016/J.JMRT.2021.07.155>.
- [7] N. Travitzky, A. Bonet, B. Dermeik, T. Fey, I. Filbert-Demut, L. Schlier, T. Schlorrdt, P. Greil, Additive manufacturing of ceramic-based materials, *Adv. Eng. Mater.* 16 (2014) 729–754, <https://doi.org/10.1002/ADEM.201400097>.
- [8] L. Wahl, M. Weichelt, N. Travitzky, Multi-material printing of reaction bonded carbides by robocasting, *Addit. Manuf.* 48 (2021) 102427, <https://doi.org/10.1016/J.ADDMA.2021.102427>.
- [9] S. Lamnini, H. Elsayed, Y. Lakhdar, F. Baino, F. Smeacetto, E. Bernardo, Robocasting of advanced ceramics: ink optimization and protocol to predict the printing parameters - a review, *Heliyon* 8 (2022) e10651, <https://doi.org/10.1016/J.HELIYON.2022.E10651>.
- [10] L. del-Mazo-Barbara, M.P. Ginebra, Rheological characterisation of ceramic inks for 3D direct ink writing: a review, *J. Eur. Ceram. Soc.* 41 (2021) 18–33, <https://doi.org/10.1016/J.JEURCERAMSOC.2021.08.031>.
- [11] J.A. Lewis, J.E. Smay, J. Stuecker, J. Cesarano, Direct ink writing of three-dimensional ceramic structures, *J. Am. Ceram. Soc.* 89 (2006) 3599–3609, <https://doi.org/10.1111/J.1551-2916.2006.01382.X>.
- [12] J.E. Smay, J. Cesarano, J.A. Lewis, Colloidal inks for directed assembly of 3-D periodic structures, *Langmuir* 18 (2002) 5429–5437, <https://doi.org/10.1021/LA0257135>.
- [13] J.I. Cesarano, T.A. Baer, P. Calvert, Recent developments in freeform fabrication of dense ceramics from slurry deposition, <https://doi.org/10.2172/554831>, 1997.
- [14] J.E. Smay, G.M. Gratson, R.F. Shepherd, J. Cesarano, J.A. Lewis, Directed colloidal assembly of 3D periodic structures, *Adv. Mater.* 14 (2002) 1279–1283, [https://doi.org/10.1002/1521-4095\(20020916\)14:18<1279::AID-ADMA1279>3.0.CO;2-A](https://doi.org/10.1002/1521-4095(20020916)14:18<1279::AID-ADMA1279>3.0.CO;2-A).
- [15] Conrad, S.R. Ferreira, J. Yoshikawa, R.F. Shepherd, B.Y. Ahn, J.A. Lewis, Designing colloidal suspensions for directed materials assembly, *Curr. Opin. Colloid Interface Sci.* 16 (2011).
- [16] E. Feilden, E.G.T. Blanca, F. Giuliani, E. Saiz, L. Vandeperre, Robocasting of structural ceramic parts with hydrogel inks, *J. Eur. Ceram. Soc.* 36 (2016) 2525–2533, <https://doi.org/10.1016/j.jeurceramsoc.2016.03.001>.
- [17] E. Feilden, D. Glymond, E. Saiz, L. Vandeperre, High temperature strength of an ultra high temperature ceramic produced by additive manufacturing, *Ceram. Int.* 45 (2019) 18210–18214, <https://doi.org/10.1016/j.ceramint.2019.05.032>.
- [18] J. Cesarano, A review of robocasting technology, *Mater. Res. Soc. Symp. Proc.* 542 (1999) 133–139, <https://doi.org/10.1557/proc-542-133>.
- [19] M.P. Sealy, G. Madireddy, R.E. Williams, P. Rao, M. Toursangsarakki, Hybrid processes in additive manufacturing, *Journal of Manufacturing Science and Engineering, Transactions of the ASME* 140 (2018), <https://doi.org/10.1115/1.4038644>.
- [20] R.W. Ford, *Drying*, MacLaren, London, [https://books.google.co.uk/books/about/Drying.html?id=LHcsAQAIAAJ&redir\\_esc=y](https://books.google.co.uk/books/about/Drying.html?id=LHcsAQAIAAJ&redir_esc=y), 1964. (Accessed 19 July 2022).
- [21] A. Ghazanfari, W. Li, M.C. Leu, G.E. Hilmas, Novel extrusion-based additive manufacturing process for ceramic parts, in: *Solid Freeform Fabrication 2016: Proceedings of the 27th Annual International Solid Freeform Fabrication Symposium*, 2016, pp. 1509–1529. [https://scholarsmine.mst.edu/mec\\_aereng\\_facwork](https://scholarsmine.mst.edu/mec_aereng_facwork).
- [22] S.E. Hall, J.E. Regis, A. Renteria, L.A. Chavez, L. Delfin, S. Vargas, M.R. Haberman, D. Espalin, R. Wicker, Y. Lin, Paste extrusion 3D printing and characterization of lead zirconate titanate piezoelectric ceramics, *Ceram. Int.* 47 (2021) 22042–22048, <https://doi.org/10.1016/j.ceramint.2021.04.224>.
- [23] A. Ghazanfari, W. Li, M.C. Leu, G.E. Hilmas, A novel freeform extrusion fabrication process for producing solid ceramic components with uniform layered radiation drying, *Addit. Manuf.* 15 (2017) 102–112, <https://doi.org/10.1016/j.addma.2017.04.001>.
- [24] B.J. Briscoe, G. Lo Biundo, N. Özkan, Drying kinetics of water-based ceramic suspensions for tape casting, [https://doi.org/10.1016/S0272-8842\(97\)00021-7](https://doi.org/10.1016/S0272-8842(97)00021-7), 1998.
- [25] Z. Fu, U. Eckstein, A. Dellert, A. Roosen, In situ study of mass loss, shrinkage and stress development during drying of cast colloidal films, *J. Eur. Ceram. Soc.* 35 (2015) 2883–2893, <https://doi.org/10.1016/j.jeurceramsoc.2015.03.029>.
- [26] J. Kiennemann, T. Chartier, C. Pagnou, J.F. Baumard, M. Huger, J.M. Lamérand, Drying mechanisms and stress development in aqueous alumina tape casting, *J. Eur. Ceram. Soc.* 25 (2005) 1551–1564, <https://doi.org/10.1016/j.jeurceramsoc.2004.05.028>.
- [27] I. Hammouda, K. Jlassi, D. Mihoubi, Changes in the physicomechanical characteristics of a ceramic paste during drying, *Compt. Rendus Mec.* 343 (2015) 419–428, <https://doi.org/10.1016/j.crme.2015.06.001>.
- [28] G.W. Scherer, Theory of drying, *J. Am. Ceram. Soc.* 73 (1990) 3–14, <https://doi.org/10.1111/j.1151-2916.1990.tb05082.x>.
- [29] Y. Itaya, H. Hanai, N. Kobayashi, T. Nakagawa, Drying-induced strain-stress and deformation of thin ceramic plate, *ChemEngineering* 4 (2020) 1–14, <https://doi.org/10.3390/chemengineering4010009>.
- [30] I. Buj-Corral, A. Domínguez-Fernández, A. Gómez-Gejo, Effect of printing parameters on dimensional error and surface roughness obtained in direct ink writing (DIW) processes, *Materials* 13 (2020), <https://doi.org/10.3390/ma13092157>.
- [31] N.P. Kim, D. Cho, M. Zielewski, Optimization of 3D printing parameters of Screw Type Extrusion (STE) for ceramics using the Taguchi method, *Ceram. Int.* (2019) 2351–2360, <https://doi.org/10.1016/j.ceramint.2018.10.152>.
- [32] Q. He, J. Jiang, X. Yang, L. Zhang, Z. Zhou, Y. Zhong, Z. Shen, Additive manufacturing of dense zirconia ceramics by fused deposition modeling via screw extrusion, *J. Eur. Ceram. Soc.* 41 (2021) 1033–1040, <https://doi.org/10.1016/J.JEURCERAMSOC.2020.09.018>.
- [33] C.L. Gnanasagaran, K. Ramachandran, S. Ramesh, S. Ubenthiran, N.H. Jamadon, Effect of co-doping manganese oxide and titania on sintering behaviour and mechanical properties of alumina, *Ceram. Int.* 49 (2023) 5110–5118, <https://doi.org/10.1016/J.CERAMINT.2022.10.027>.
- [34] J. Hinton, D. Basu, D.F. Flynn, R.A. Harris, R.W. Kay, A digitally-driven Hybrid Manufacturing process for the flexible production of engineering ceramic components, in: *Solid Freeform Fabrication 2018: Proceedings of the 29th Annual International Solid Freeform Fabrication Symposium*, 2018, in: [https://www.researchgate.net/publication/333104494\\_A\\_digitally-driven\\_Hybrid\\_Manufacturing\\_process\\_for\\_the\\_flexible\\_production\\_of\\_engineering\\_ceramic\\_components](https://www.researchgate.net/publication/333104494_A_digitally-driven_Hybrid_Manufacturing_process_for_the_flexible_production_of_engineering_ceramic_components). (Accessed 23 February 2022).
- [35] W. Li, A. Ghazanfari, M.C. Leu, R.G. Landers, Extrusion-on-demand methods for high solids loading ceramic paste in freeform extrusion fabrication, *Virtual Phys. Prototyp.* (2017), <https://doi.org/10.1080/17452759.2017.1312735>.
- [36] M.S. Mason, T. Huang, R.G. Landers, M.C. Leu, G.E. Hilmas, Aqueous-based extrusion of high solids loading ceramic pastes: process modeling and control,

- J. Mater. Process. Technol. 209 (2009) 2946–2957, <https://doi.org/10.1016/J.JMATPROTEC.2008.07.004>.
- [37] supermerril, SuperSlicer v2.5.59.2. <https://github.com/supermerill/SuperSlicer/tree/2.5.59.2>, 2023. (Accessed 4 December 2023).
- [38] S.G. Kwak, J.H. Kim, Central limit theorem: the cornerstone of modern statistics, Korean J Anesthesiol 70 (2017) 144–156, <https://doi.org/10.4097/kjae.2017.70.2.144>.